Supplementary Materials for

# Improving electronegativity of N-doped carbon by encapsulating CoFe alloy clusters with a chainmail-like structure for high-energy sodium-ion capacitors

Zhao Li*[a], Rui Wu[b], Zhaozhao Zhu [b], Ying Zhu [b], Yamei Wang [b], Shilong Xu [b], Qingquan Kong [a] and Jun Song Chen*[a,b]

[a] *Institute for Advanced Study, Chengdu University, Chengdu 610106, China. E-mail: lizhao2019@cdu.edu.cn; jschen@uestc.edu.cn*

[b] *School of Materials and Energy, University of Electronic Science and Technology of China, Chengdu 610054, China.*

# 1. Experimental Section

*1.1 Materials and reagents*

Zinc nitrate hexahydrate ($Zn(NO_3)_2 \cdot 6H_2O$, 98%), Cobalt nitrate hexahydrate ($Co(NO_3)_2 \cdot 6H_2O$, 98%), 2-Methylimidazole (2-MeIM, 99%), and iron acetylacetonate ($Fe(acac)_3$, 98%) were bought from Aladdin. Dimethylformamide (DMF, 99.9%), polyacrylonitrile (PAN, average MW 150,000).

*1.2 Synthesis of Fe-N-C and porous nitrogen-dopes carbon nanofiber (PNCF)*

Fe-N-C and porous nitrogen-dopes carbon nanofiber (PNCF) were synthesized by our previously reported work.[1] Firstly, ZIF-8 and Fe doped ZIF-8 nanoparticles (NPs) were prepared as our previously reported method. After that, 300 mg of as-prepared Fe/Zn-ZIF-8 NPs and 300 mg of PAN were added to 3.55 mL of DMF solvent and stirred for 24 h to form a homogeneously dispersed solution. The mixture was then transferred to a plastic syringe (10 mL) for electrospinning using a stainless steel needle connected to a high-voltage DC power (17 kV). The solution flow rate and the distance between the needle and the Al foil collector were 1.2 mL $h^{-1}$ and 17 cm, respectively. Finally, the obtained Fe/Zn-ZIFs/PAN composites were dried overnight at 60 °C under vacuum. For comparison, Zn-ZIFs/PAN precursors were synthesized by a similar procedure with adding ZIF-8 NPs. The obtained Fe/Zn-ZIFs/PAN and Zn-ZIFs/PAN composites were firstly pre-oxidized in air at 220 °C for 2 h and immediately pyrolyzed under argon at 900 °C for 2 h. Finally, the Fe-N-C and PNCF were obtained.

*1.3 Synthesis of CoFe-N-C and Co-N-C*

Co-ZIFs NPs were synthesized by a modified method. 3.70 g of 2-methylimidazole was dissolved in 80 mL of methanol to form a clear solution and then mixed with 80 mL of methanol solution containing 1.606 g of $Zn(NO_3)_2 \cdot 6H_2O$ and 78 mg of $Co(NO_3)_2 \cdot 6H_2O$. After vigorous stirring for 1 h, the mixture was rested at room temperature with a standing time of 12 h. The resulting precipitate was collected by centrifugation and washed by methanol for three times. After drying in vacuum at 60 °C for 12 h, the final product with purple color was obtained. For Fe-doped Co-ZIFs NPs (Fe/Co-ZIFs), 200 mg of as-prepared Co-ZIFs NPs and 40 mg $Fe(acac)_3$ were dispersed into 20 mL of ethanol for continuously stirring for 24 h. Fe/Co-ZIFs NPs were obtained after centrifugation and drying in a vacuum oven at 60 °C overnight. The final sample of CoFe-N-C and Co-N-C were prepared by a similar procedure like Fe-N-C with adding Fe/Co-ZIFs NPs or Co-ZIFs NPs.

## 2. Characterization

The morphologies of the as-prepared samples were observed using SEM (Phenom Pharos), and TEM (JEM2010F). XRD pattern characterization was performed on a Areis using Cu Kg radiation. Raman spectra were analyzed using a laser confocal instrument (Renishaw Invia). Inductively coupled plasma optical emission spectrometry (ICP-OES) was performed on Agilent 720ES. X-ray photoelectron spectroscopy (XPS) was performed using a Thermo Fisher Scientific, Escalab 250Xi with AI Kα radiation.

**3. Electrochemical Measurements**

The sodium storage performance were tested using CR2032 coin-type cells. The active material, and polyvinylidene difluoride (PVDF) were mixed at a weight ratio of 9:1 by hand milling with N-methyl pyrrolidinone to obtain a homogeneous slurry. Subsequently, the slurry was coated on copper foil and vacuum dried at 60 °C for 2 h. The loading mass of active materials on the current collector is about 0.6-0.9 mg $cm^{-2}$. All the cells were assembled in a glovebox filled with argon. For half-cell tests, a Na foil was used as the counter and reference electrode, and the glass fiber (GF/D) from Whatman were used as the separator and the electrolyte was 1 M $NaPF_6$ dissolved in Dimethyl Ether. The electrochemical measurements of anodes were conducted between 0.01 V and 3.0 V (versus $Na/Na^+$).

For the full cell SICs devices, PNCF was used as the cathode material using the same method except for the aluminum foil current collector and 1 M $NaPF_6$ in Dimethyl Ether as the electrolyte. For the sake of boosting the electrochemical performances (cycling stability, energy, and power density) of this CoFe-N-C//PNCF SICs device, an pre-sodium strategy was applied to solve the issues of low ICE and appropriate mass ratio of cathode to anode (3:1) was adopt to relieve specific capacity imbalance between anode and cathode electrodes. To pre-sodium the anode, it was initially discharged and charged at 0.1 A $g^{-1}$ for 6 cycles and finally discharged to 0.01 V in a half-cell before assembling the SICs. And then, we carefully disassembled this battery and taken out the anode to assemble the SICs devices. It is not needed to clean or dry process for the pre-sodiated anode because of same electrolyte and the separator was used for next assembling the SICs. The preactivated CoFe-N-C and the as-prepared PNCF cathode

were then used to construct the SICs devices, with the mass ratios of the anode and cathode fixed at 1:3. For the full cell test, CV and galvanostatic charge/discharge (GCD) were carried out at a broad working voltage window between 0-4.0 V. The galvanostatic charge/discharge tests were performed on a Neware battery tester. Cyclic voltammetry (CV) was carried out on a Bio-logic SP-150 electrochemical workstation. Electrochemical impedance spectroscopy (EIS) was carried out on a BioLogic electrochemical workstation by applying an AC voltage with 5 mV amplitude in a frequency range from $10^5$ Hz to 0.1 Hz.

The energy and power density could be calculated using the under equations:

$$P = \Delta V \times I / m \qquad (1)$$

$$\Delta V = (V_{max} + V_{min}) / 2 \qquad (2)$$

$$E = \int_{t1}^{t2} /V \bullet dt = \frac{1}{2} C(V_{max} + V_{min})(V_{max} - V_{min}) = \frac{V_{max} + V_{min}}{2} \times \frac{I \times t}{m} \times \frac{1}{3.6} \qquad (3)$$

where $V_{max}$ and $V_{min}$ are the voltages at beginning and end of discharge; I is the discharge current; m is based on the total mass of active materials containing cathode and anode; t is the discharge time.

**4. Density functional theory (DFT) computational details**

All simulations were carried out on Vienna Ab-initio Simulation Package (VASP)[2] based on the density functional theory (DFT).[3] The projected augmented wave (PAW) was adopted to describe the ion-electron interactions.[4] The perdew-Burke-Ernzerhof (PBE) functional was employed to describe the electron-electron interaction.[5] An energy cutoff of 450 eV was used, and a k-point sampling set of 2 × 2 × 1 was tested to

be converged. The vacuum space was set to be 20 Å to avoid the interaction between adjacent layers.

**Supplementary Figures**

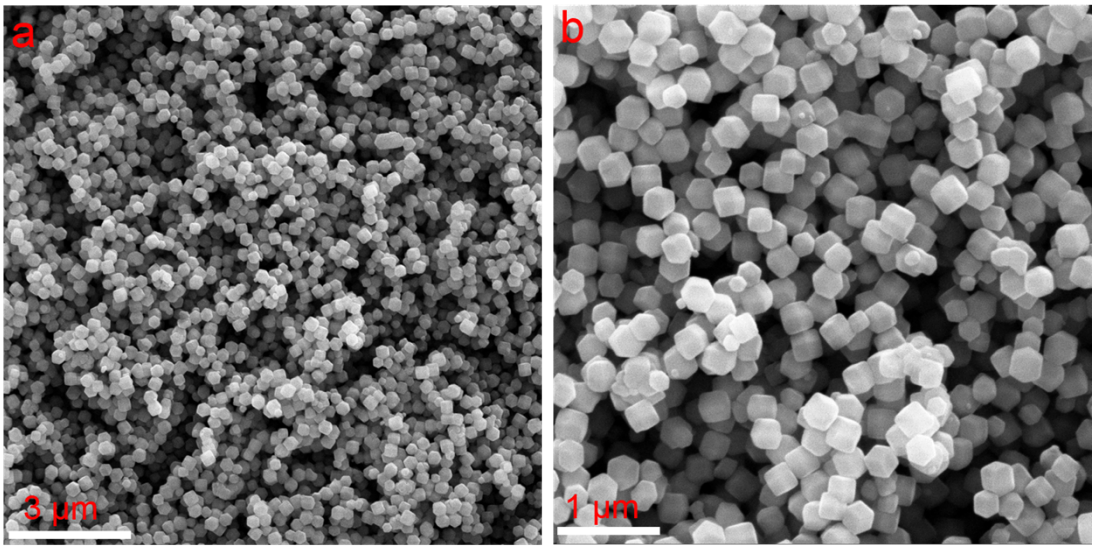


**Figure S1.** SEM images of Fe/Co-ZIFs at different magnifications.

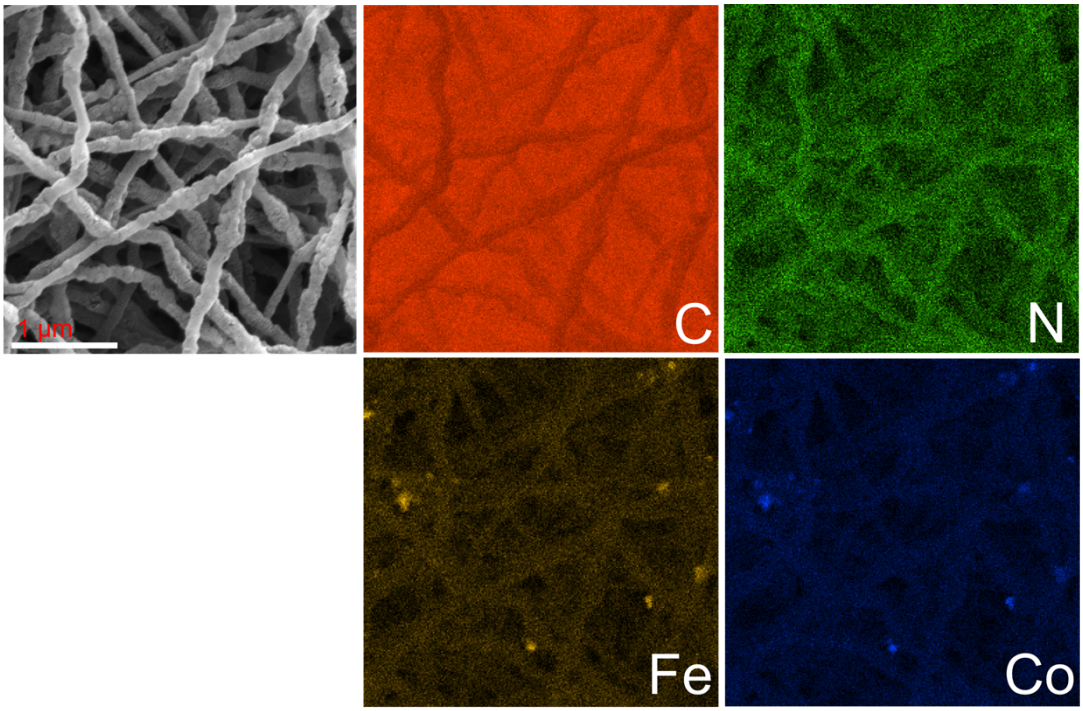


**Figure S2.** SEM image and energy dispersive X-ray spectroscopy (EDX) elemental mapping of FeCo-N-C.

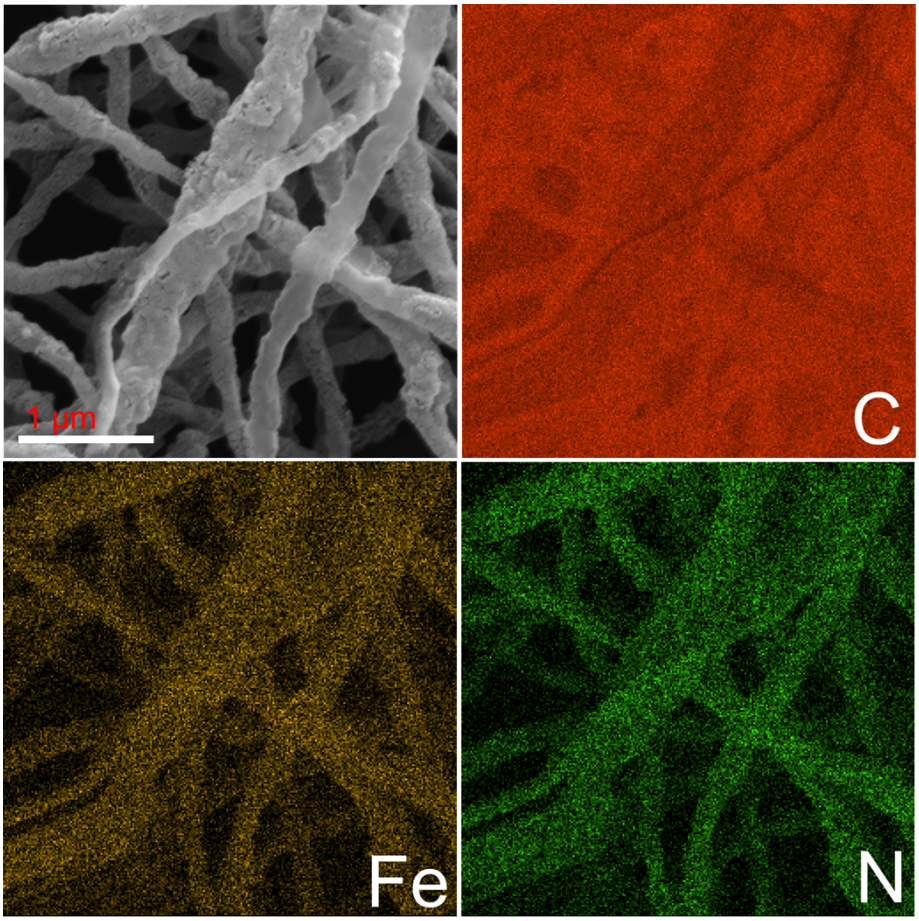


**Figure S3.** SEM image and energy dispersive X-ray spectroscopy (EDX) elemental mapping of Fe-N-C.

.

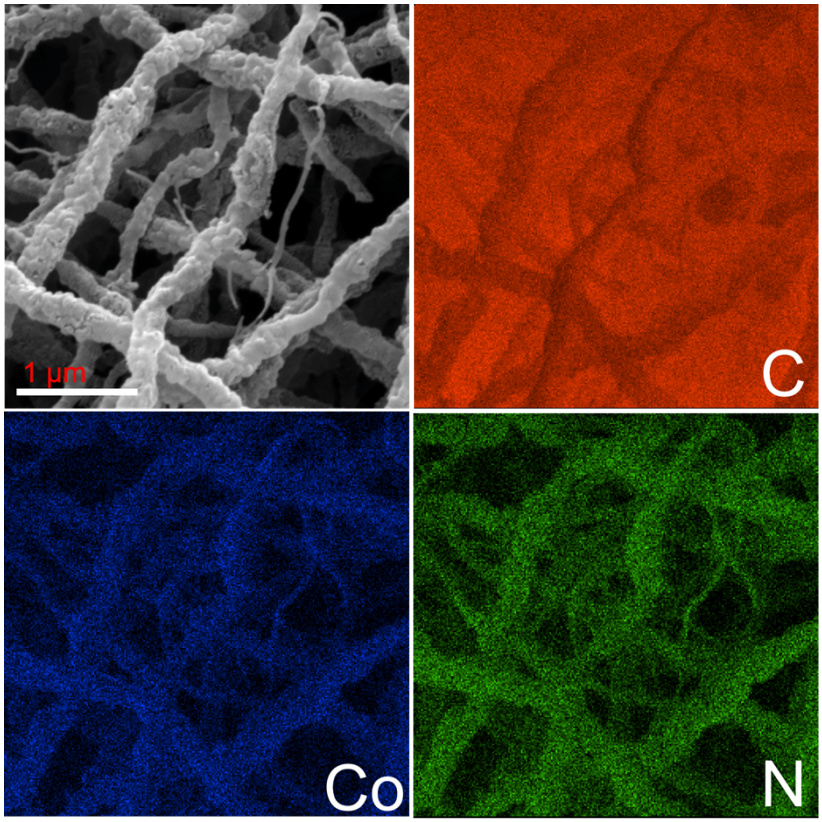


**Figure S4.** SEM image and energy dispersive X-ray spectroscopy (EDX) elemental mapping of Co-N-C.

.

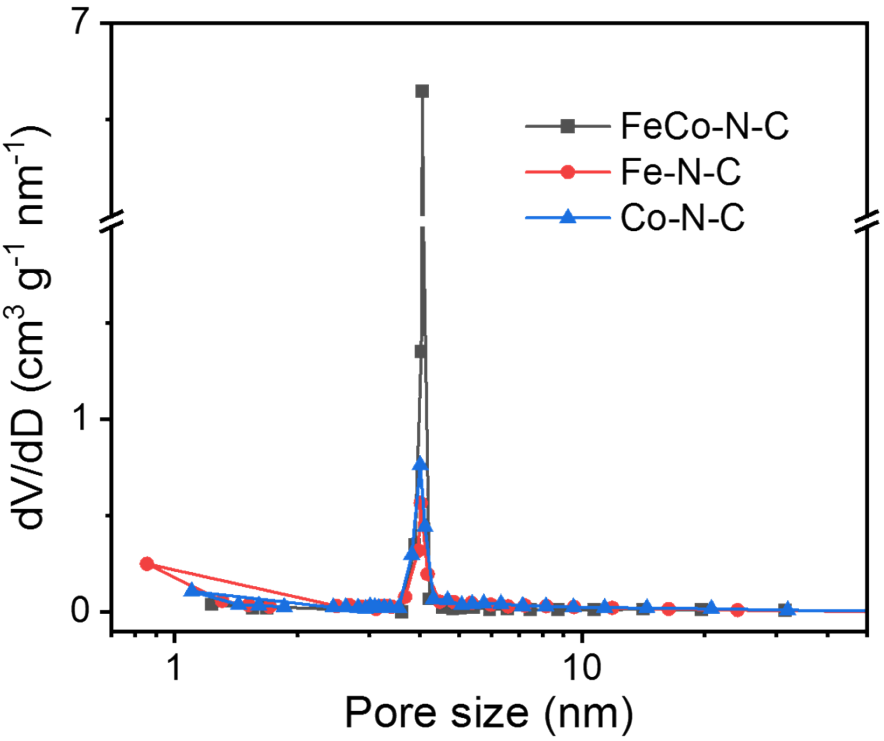


**Figure S5.** Pore size distribution curves of Co-N-C, Fe-N-C, and FeCo-N-C.

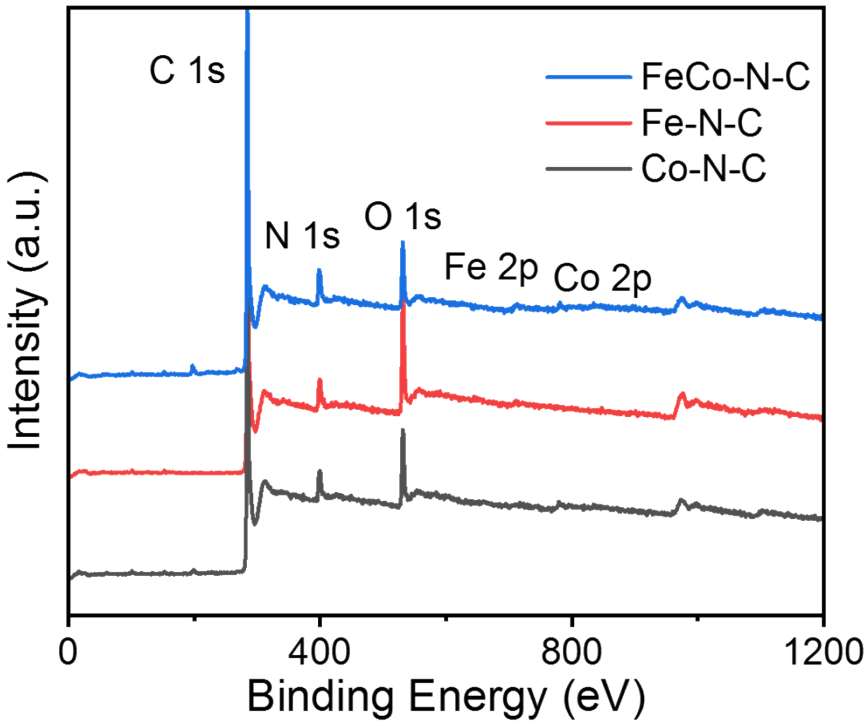


**Figure S6.** XPS survey spectra of Co-N-C, Fe-N-C, and FeCo-N-C.

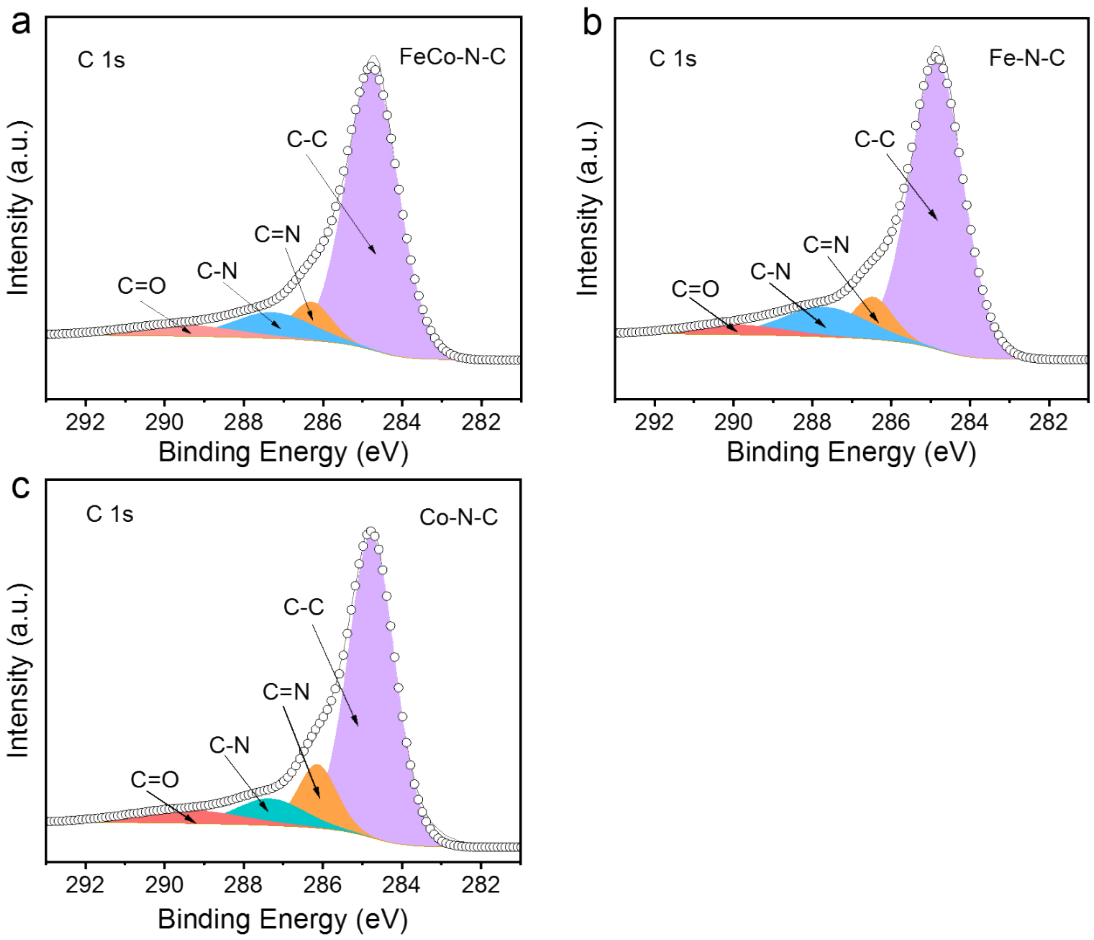


**Figure S7.** High-resolution C 1s XPS spectra of (a) FeCo-N-C, (b) Fe-N-C, and (c) Co-N-C.

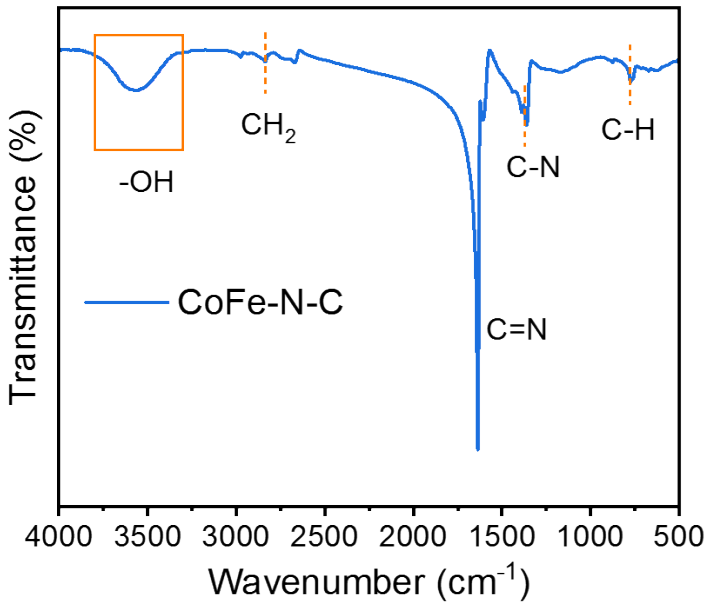


**Figure S8.** FTIR for CoFe-N-C.

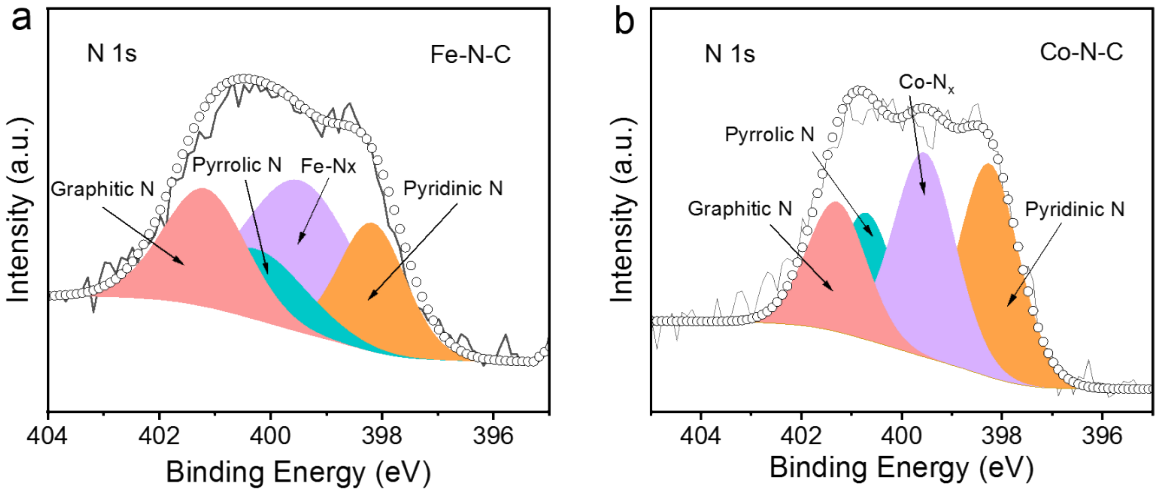


**Figure S9.** High-resolution N 1s XPS spectra of (a) Fe-N-C and (b) Co-N-C.

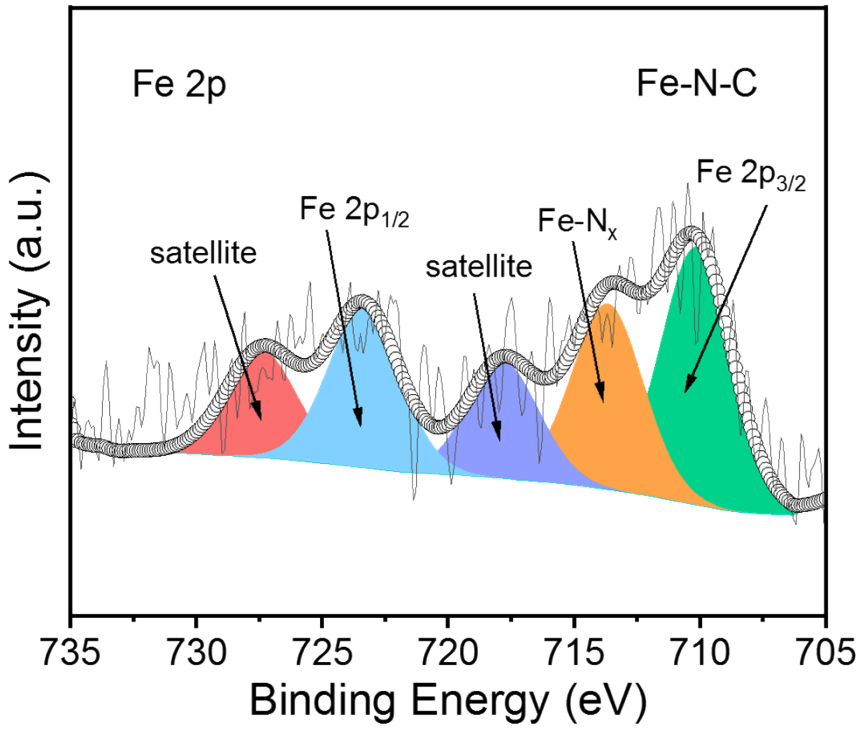


**Figure S10.** High-resolution Fe 2p XPS spectra of Fe-N-C.

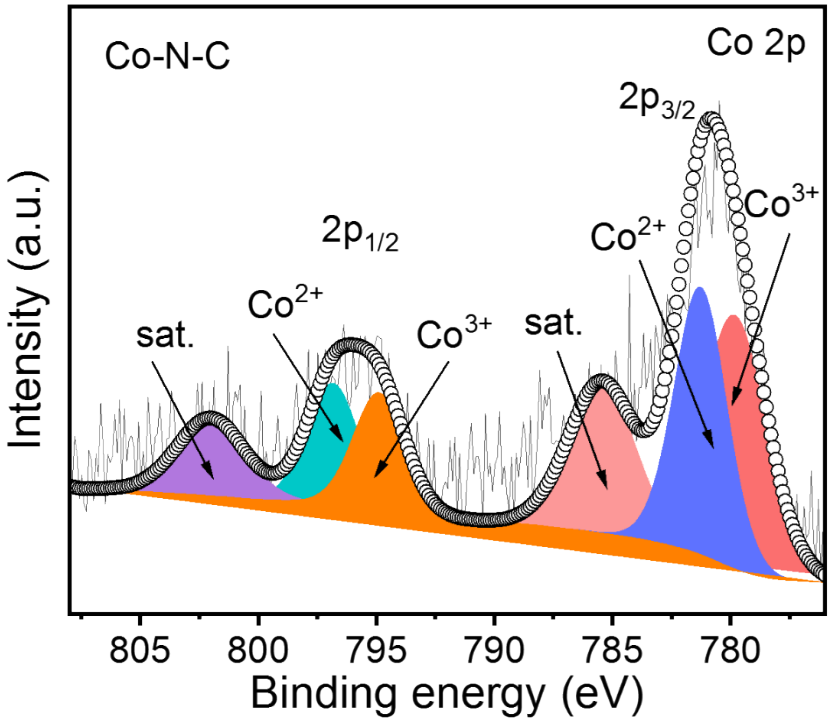


**Figure S11.** High-resolution Co 2p XPS spectra of Co-N-C.

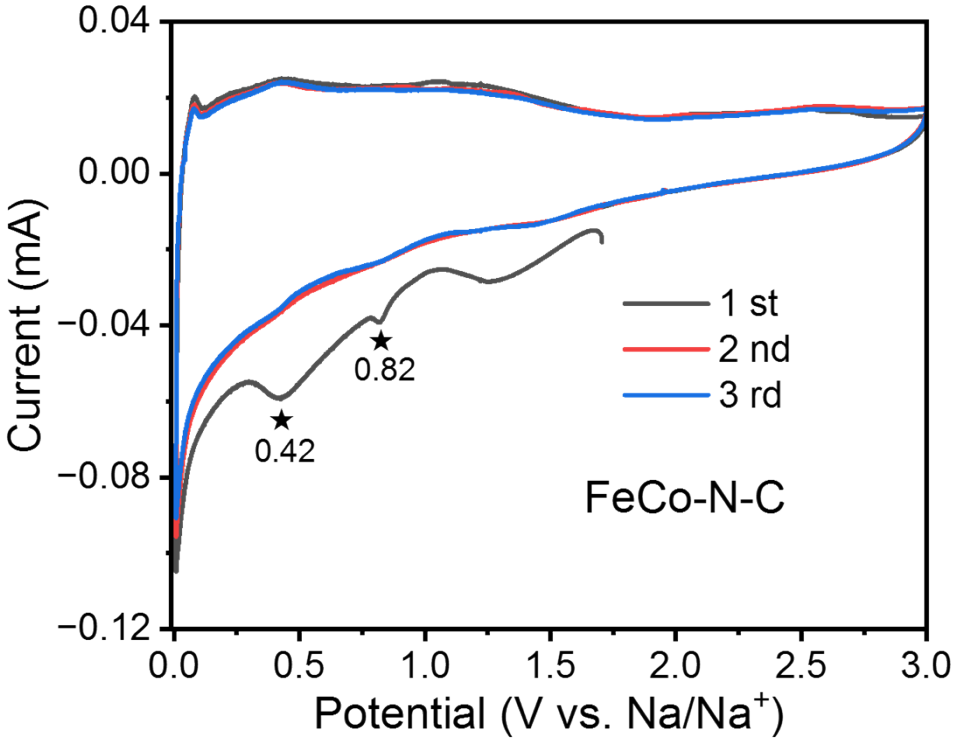


**Figure S12.** Typical CV curve of CoFe-N-C sample as anode at a scan rate of 0.1 mV $s^{-1}$ for initial three cycles.

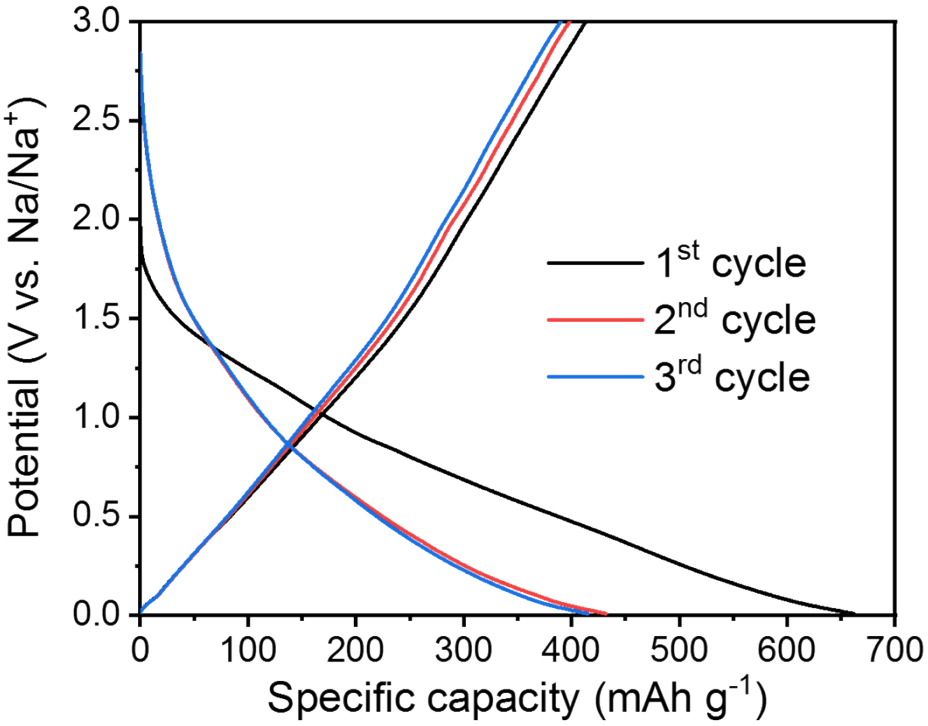


**Figure S13.** Galvanostatic charge-discharge curve of CoFe-N-C sample as anode at a current density of 0.1 A $g^{-1}$ for initial three cycles.

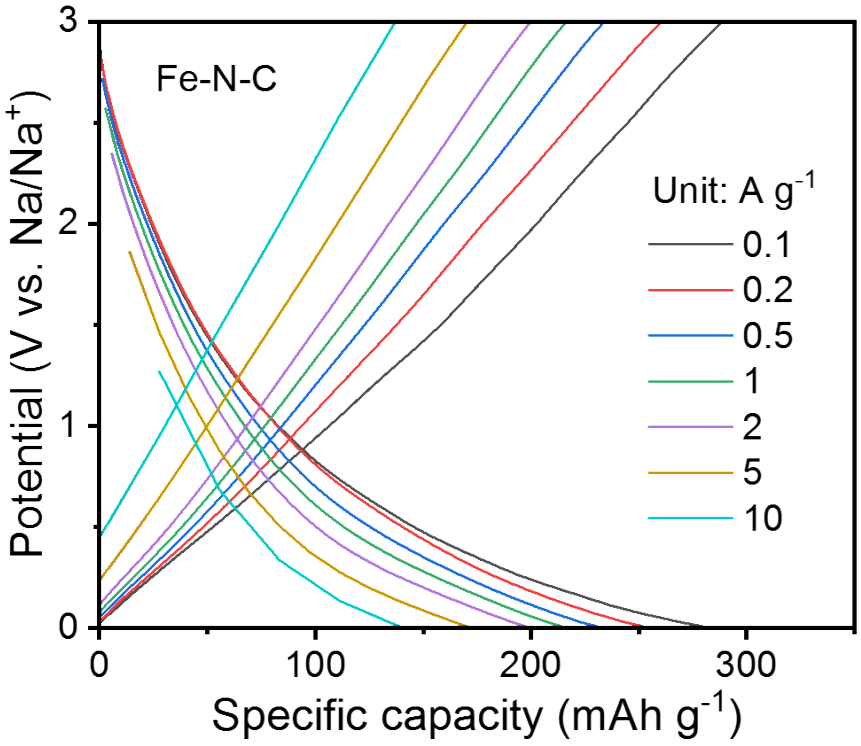


**Figure S14.** Charge-discharge curves of the Fe-N-C sample as anode electrode at different current densities.

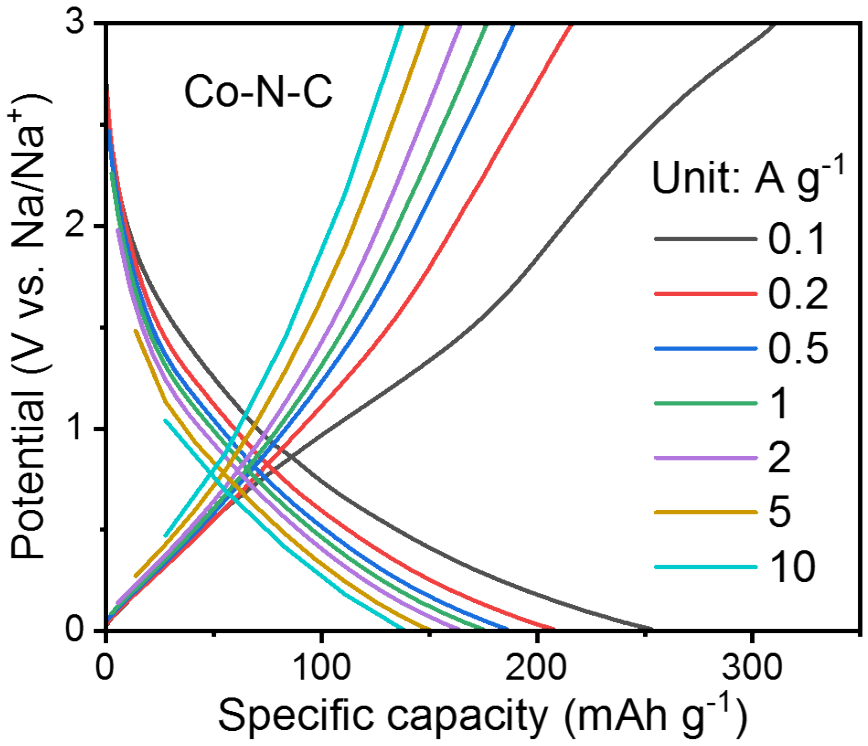


**Figure S15.** Charge-discharge curves of the Co-N-C sample as anode electrode at different current densities.

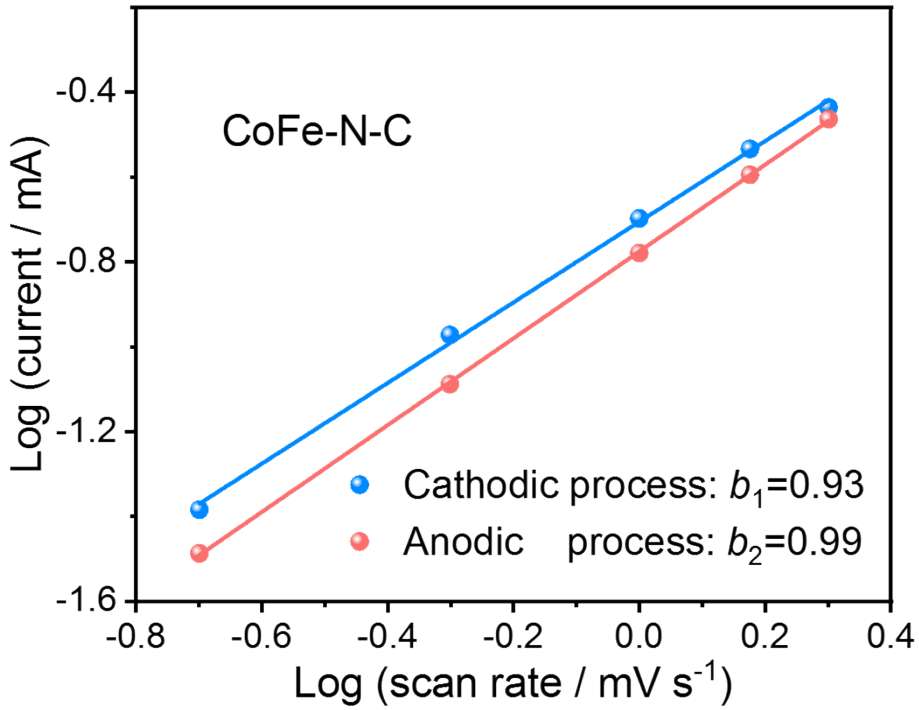


**Figure S16.** Relationships between peak current and sweep rate of CoFe-N-C with estimated b values.

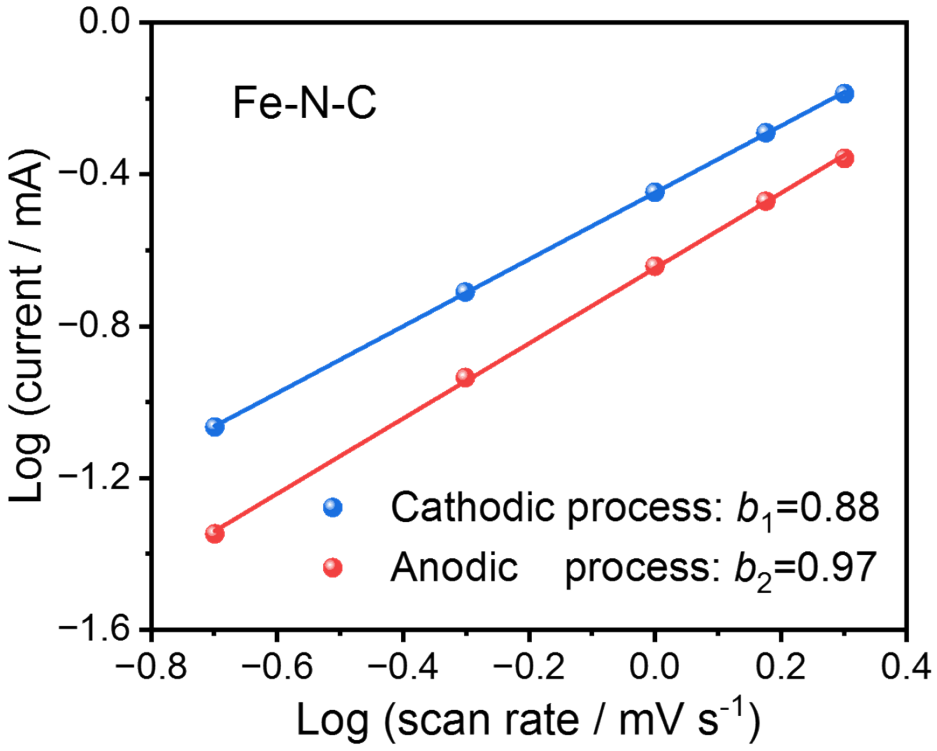


**Figure S17.** Relationships between peak current and sweep rate of CoFe-N-C with estimated b values.

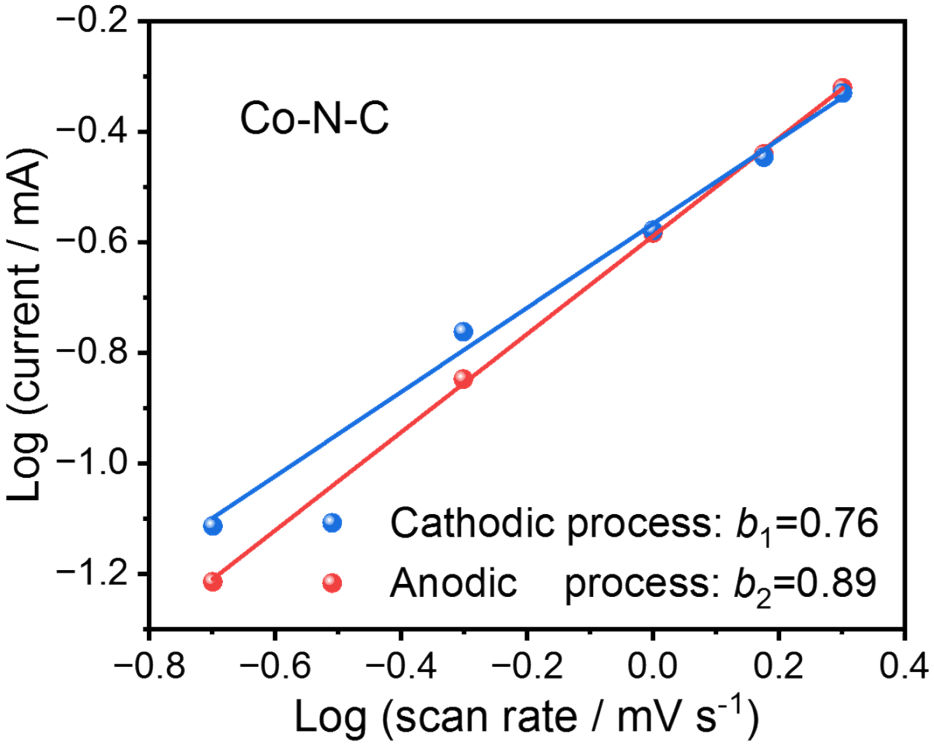


**Figure S18.** Relationships between peak current and sweep rate of CoFe-N-C with estimated b values.

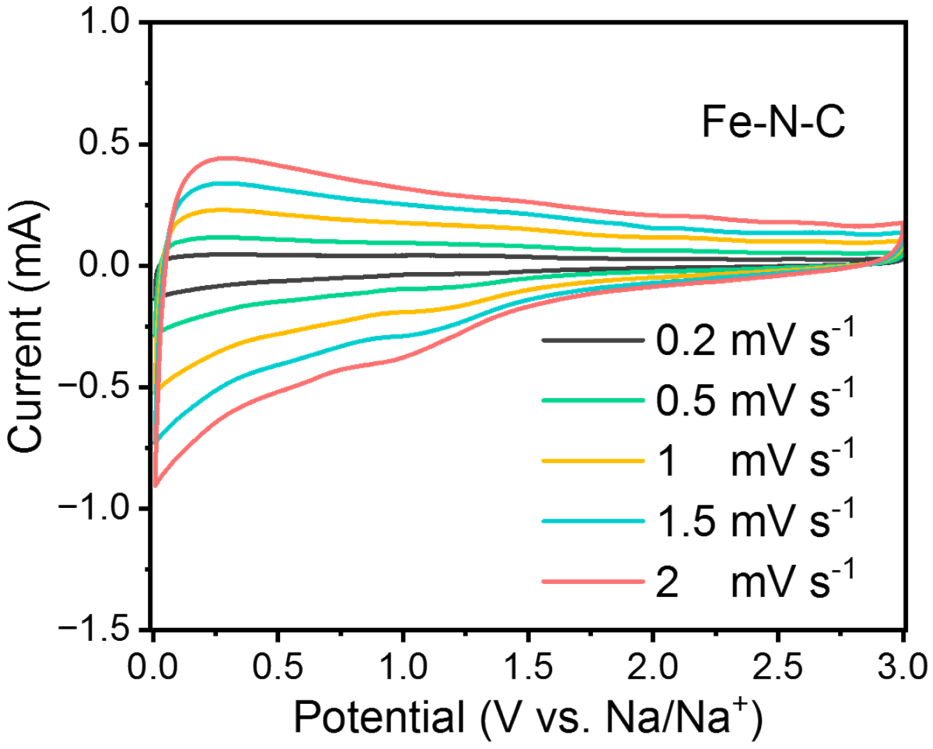


**Figure S19.** CV curves of the Fe-N-C sample as electrode at different scan rates.

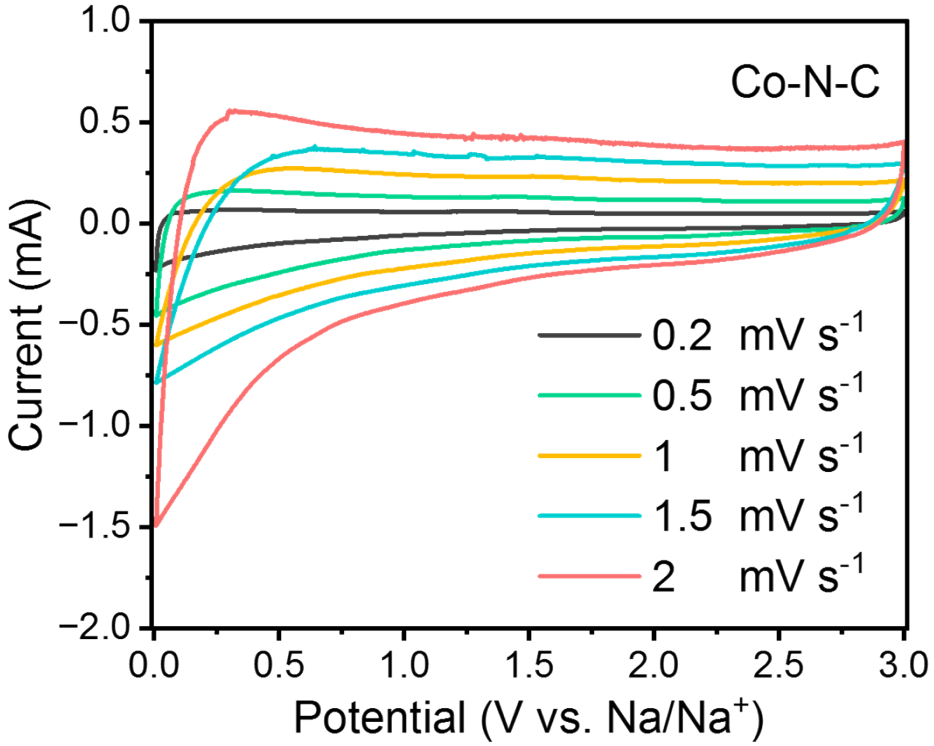


**Figure S20.** CV curves of the Co-N-C sample as electrode at different scan rates.

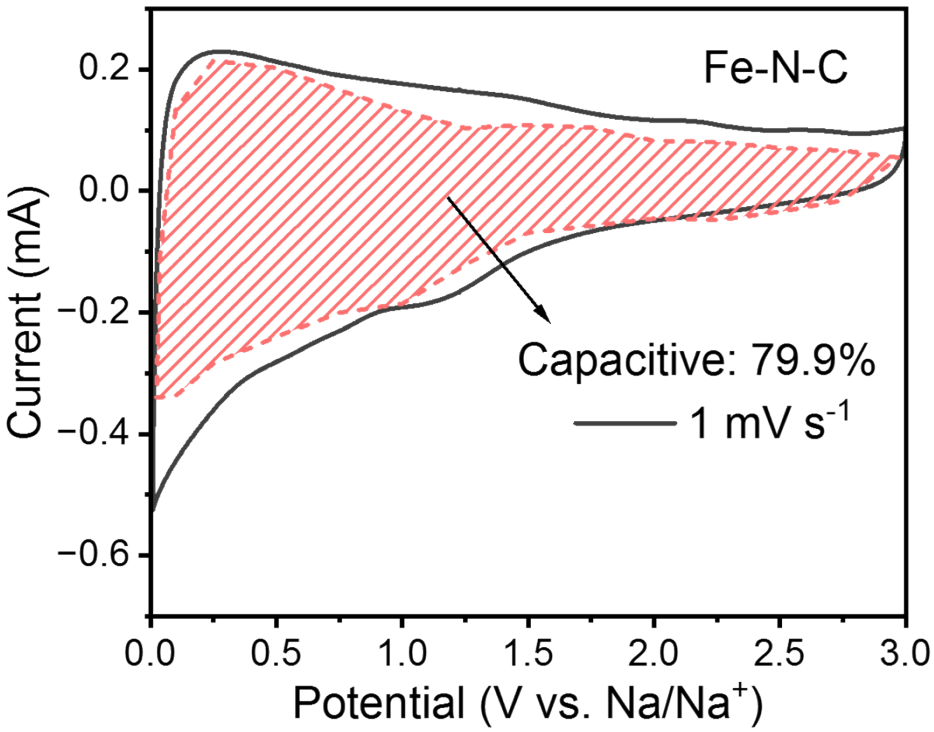


**Figure S21.** The surface capacitive contribution of the Fe-N-C sample as anode electrode obtained from the CV curve of 1 mV $s^{-1}$ (shadowed area).

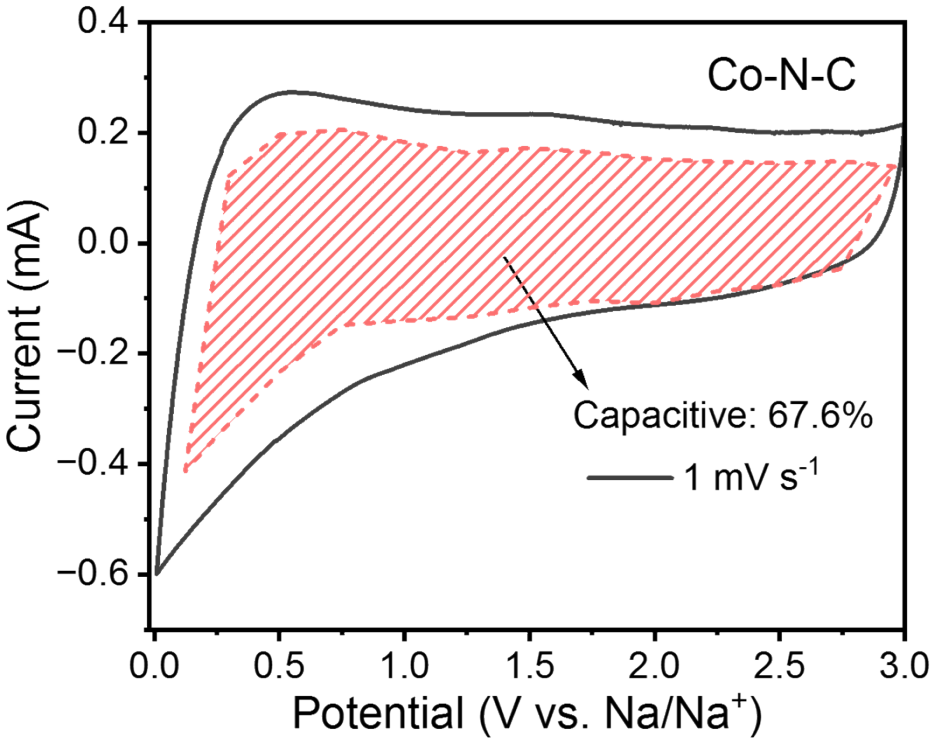


**Figure S22.** The surface capacitive contribution of the Co-N-C sample as anode electrode obtained from the CV curve of 1 mV $s^{-1}$ (shadowed area).

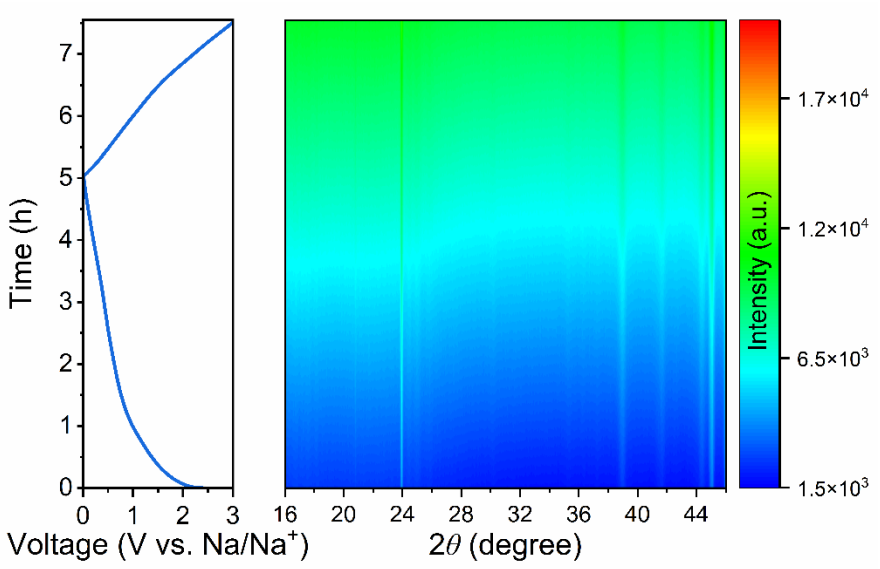


**Figure S23.** *In situ* XRD patterns of CoFe-N-C characterized during the initial discharge/charge cycle.

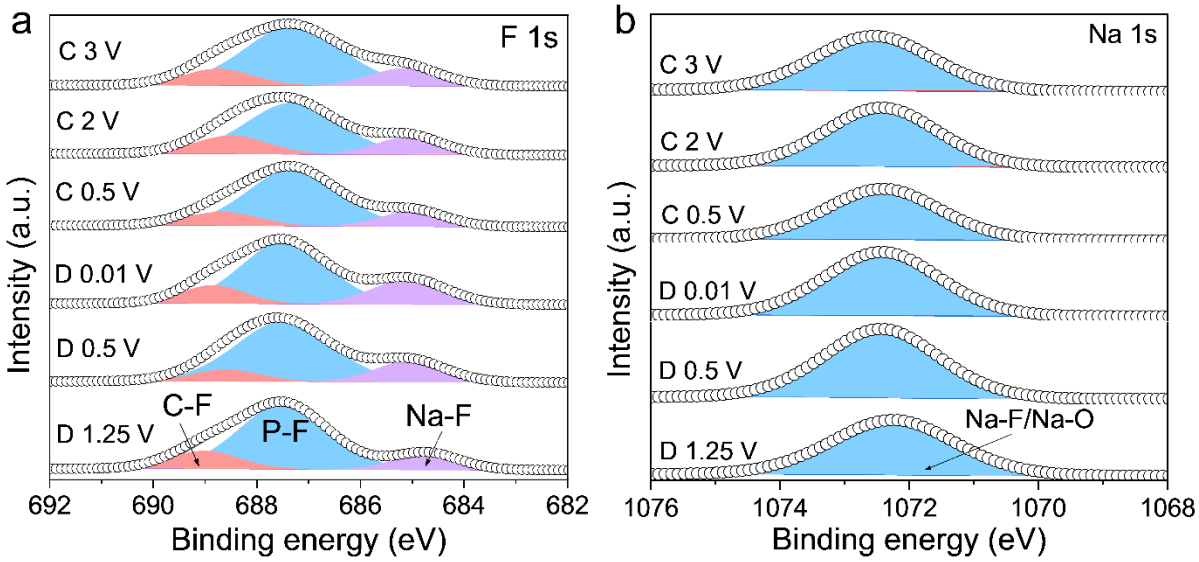


**Figure S24.** *Ex-situ* XPS spectra of (a) F 1s and (b) Na 1s in CoFe-N-C anodes at different states (D: state of discharge, C: state of charge).

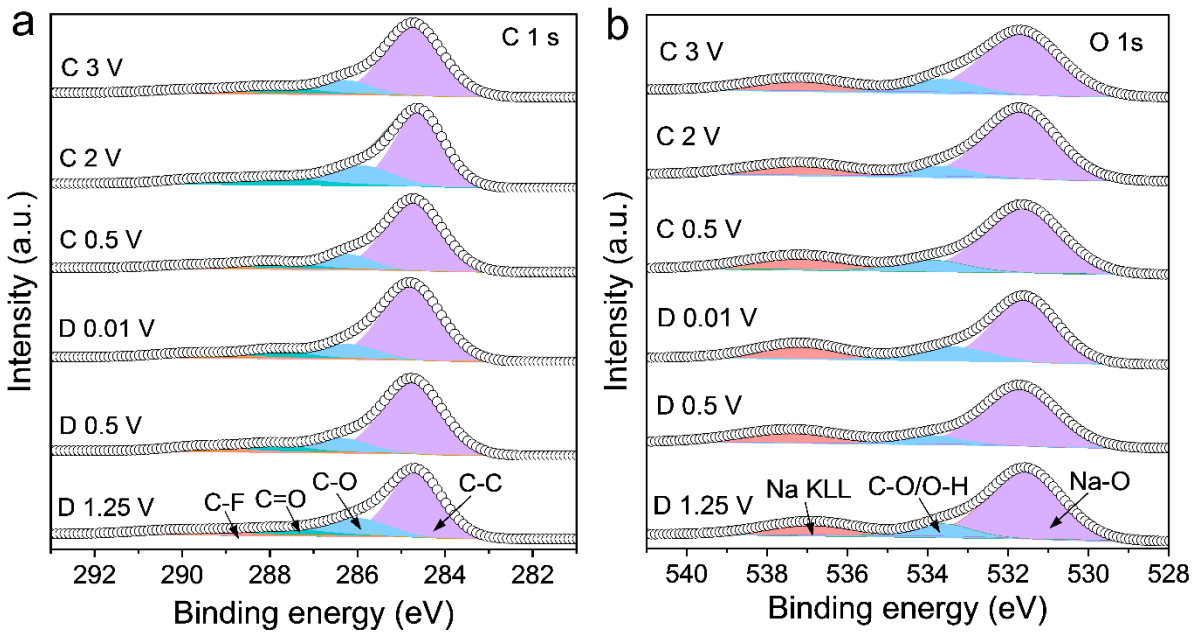


**Figure S25.** *Ex-situ* XPS spectra of (a) C 1s and (b) O 1s in CoFe-N-C anodes at different states (D: state of discharge, C: state of charge).

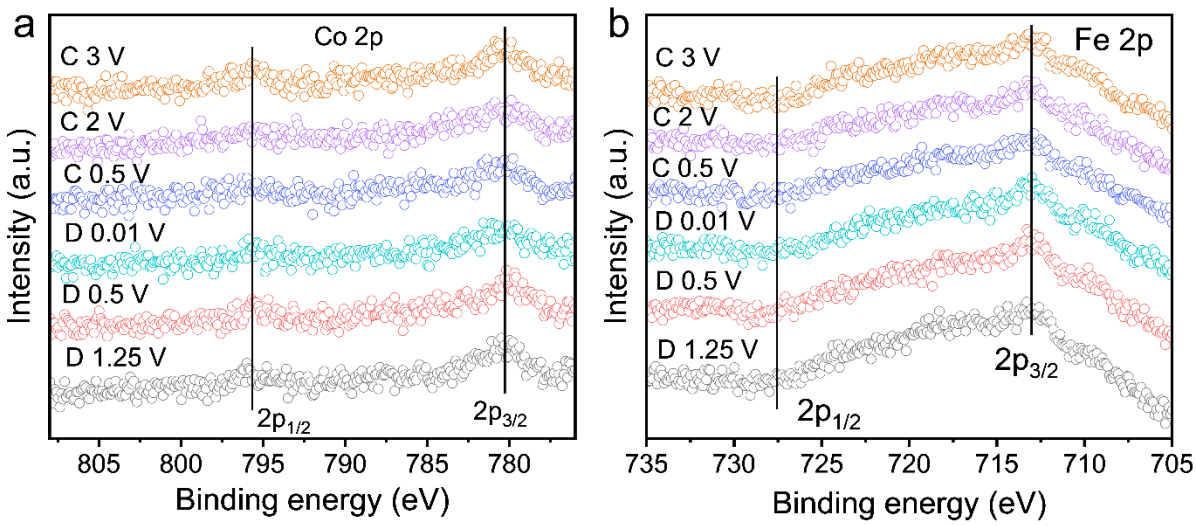


**Figure S26.** *Ex-situ* XPS spectra of (a) Co 2p and (b) Fe 2p in CoFe-N-C anodes at different states (D: state of discharge, C: state of charge).

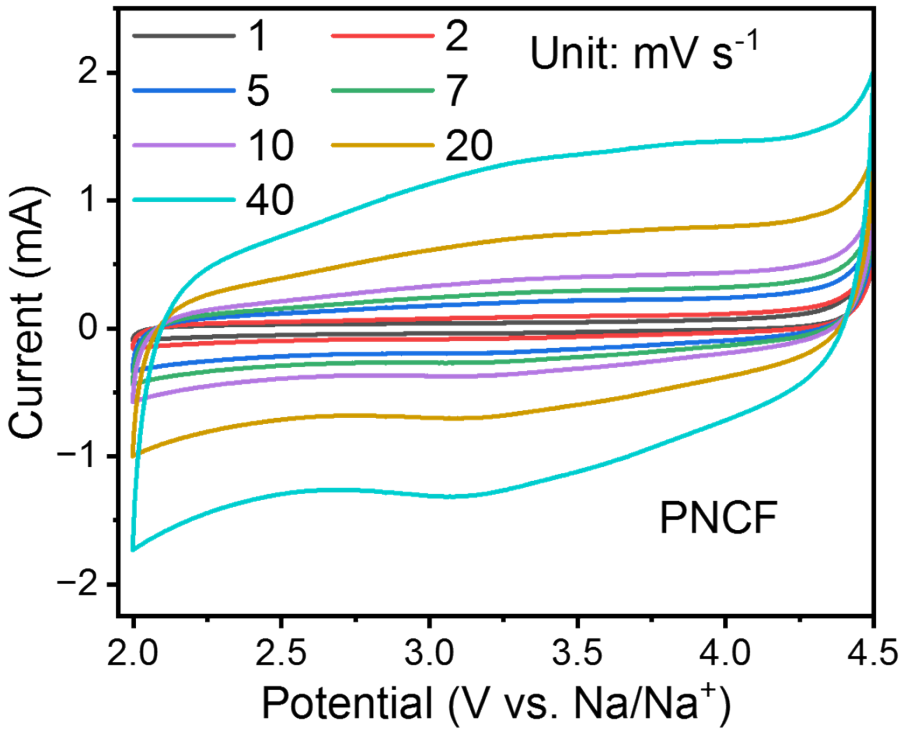


**Figure S27.** CV curves of the PNCF sample as cathode at different scan rates (from 1 to 40 mV $s^{-1}$).

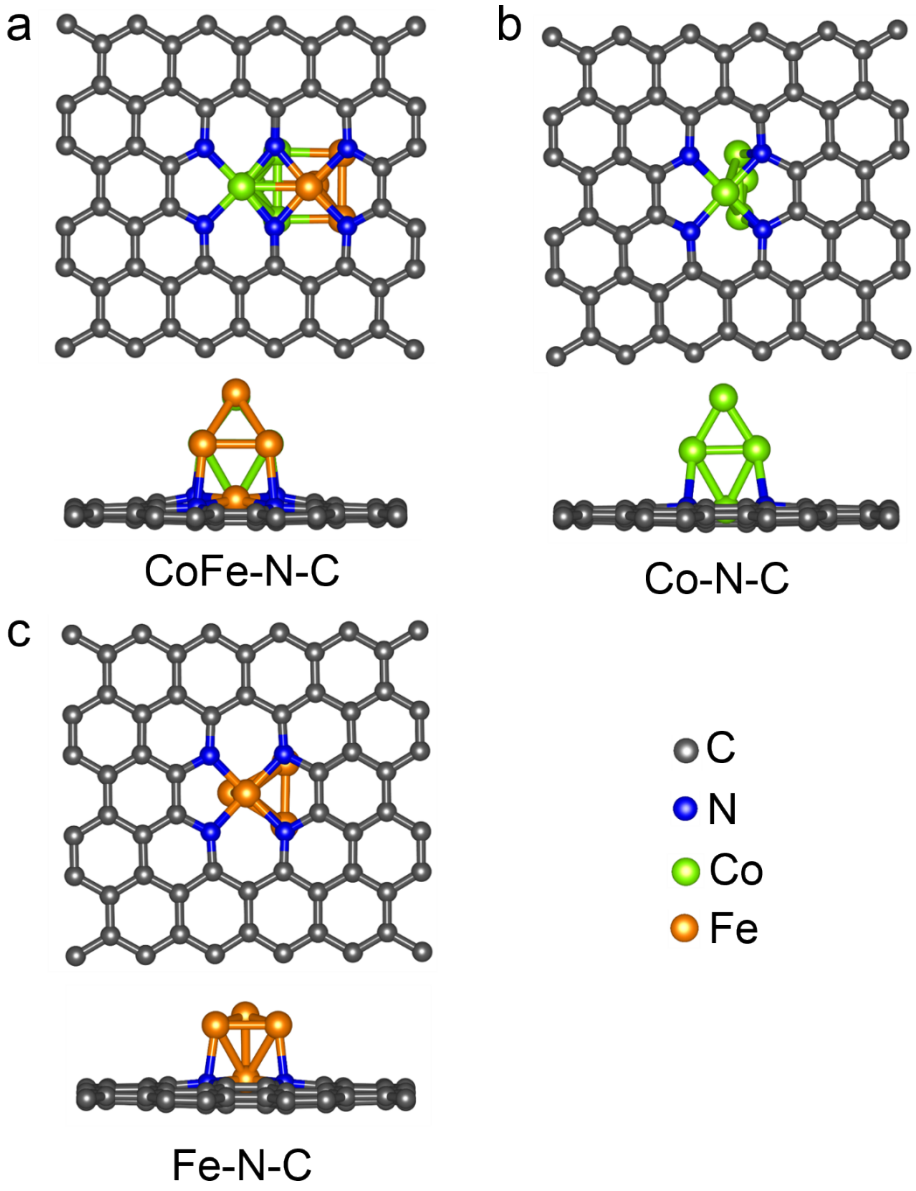


**Figure S28.** The optimized structures for (a) CoFe-N-C, (b) Co-N-C, and (c) Fe-N-C models.

**Table S1.** Summaries of BET specific surface area, pore diameter, pore volume, and $I_D/I_G$ for the Fe-N-C, Co-N-C, and CoFe-N-C samples.

| Samples | $S_{BTE}$ ($m^2$ $g^{-1}$) | Average pore diameter (nm) | Pore volume ($cm^3$ $g^{-1}$) | $I_D/I_G$ |
|---|---|---|---|---|
| Fe-N-C | 453 | 3.52 | 0.80 | 0.93 |
| Co-N-C | 384 | 4.83 | 0.93 | 0.94 |
| CoFe-N-C | 230 | 6.73 | 6.73 | 0.97 |

**Table S2.** The element contents (atomic %) and peak quantification of XPS fitted N1s spectra.

| Samples | C | N | Co | Fe | Pyrrolic N | M-$N_x$ | Pyridinic N | Graphitic N |
|---|---|---|---|---|---|---|---|---|
| Fe-N-C | 91.57 | 7.96 | / | 0.47 | 16.9 | 39.7 | 20.3 | 23.1 |
| Co-N-C | 92.56 | 7.04 | 0.39 | / | 17.4 | 31.6 | 31.7 | 19.3 |
| CoFe-N-C | 90.88 | 8.14 | 0.42 | 0.56 | 28.4 | 32.4 | 24.6 | 14.6 |

**Table S3.** Comparison of the results in our study with those previously reported carbon-based anode in half cell for sodium ion storage.

| Samples | Voltage window | ICE | Current density | Cycle number | Capacity (mAh $g^{-1}$) | Capacity retention | Ref |
|---|---|---|---|---|---|---|---|
| CoFe-N-C | 0.01-3 V | 62.5% | 1 A $g^{-1}$ | 3000 | 298 | ~100% | This work |
| S-N-CBFs | 0.01-3 V | 51.4% | 1 A $g^{-1}$ | 3500 | 257 | ~100% | [6] |
| N-CBFs | 0.01-3 V | 40.5% | 1 A $g^{-1}$ | 3500 | 185 | ~100% | [6] |
| PCNS | 0.01-3 V | 29% | 0.5 A $g^{-1}$ | 5000 | 205 | ~100% | [7] |
| OMC | 0.01-3 V | 19.9% | 1 A $g^{-1}$ | 3000 | 150 | 85.6% | [8] |
| PFHC-20 | 0.01-3 V | 84.7% | 0.1 A $g^{-1}$ | 300 | 196.9 | 85% | [9] |

**Table S4.** Fitting results of EIS in Figure 3 with the proposed equivalent circuit.

| **Samples** | **$R_S$ (Ω)** | **$R_{CT}$ (Ω)** |
|---|---|---|
| Co-N-C | 2.1 | 103.9 |
| Fe-N-C | 10.0 | 100.0 |
| CoFe-N-C | 12.4 | 55.8 |

**Table S5.** The energy densities and power densities of our CoFe-N-C//PNCF SICs device at different current densities.

| Samples | 0.1 | 0.2 | 0.5 | 1 | 2 | 5 | 10 |
|---|---|---|---|---|---|---|---|
| Powder density (W $kg^{-1}$) | 200 | 400 | 1000 | 2000 | 4000 | 10000 | 20000 |
| Energy density (Wh $kg^{-1}$) | 211.6 | 209.8 | 193.3 | 187.2 | 173.2 | 153.6 | 127.8 |

**Table S6.** Comparison of previously reported SICs devices with our CoFe-N-C//PNCF SICs device.

| SICs Anode//Cathode | Energy density | Power density | Stability and Voltage window | Ref |
|---|---|---|---|---|
| CoFe-N-C//PNCF | 211.6 Wh $kg^{-1}$ at 200 W $kg^{-1}$ | 20 kW $kg^{-1}$ at 127 Wh $kg^{-1}$ | 88.4% after 900 cycles at 1 A $g^{-1}$ 0-4 V | This work |
| TH-HCS//AC | 106.1 Wh $kg^{-1}$ at 409 W $kg^{-1}$ | 8.19 kW $kg^{-1}$ at 46.6 Wh $kg^{-1}$ | 81.1% after 5000 cycles at 1 A $g^{-1}$ 0.01-3.8 V | 10 |
| $Co_xTi_{1-x}O_y$//AC | 164 Wh $kg^{-1}$ at 31 W $kg^{-1}$ | 8.307 kW $kg^{-1}$ at 56 Wh $kg^{-1}$ | 83% after 15000 cycles at 1 A $g^{-1}$ 0-4 V | 11 |
| $Co_2P$/Sn@NC//PAC | 112.3 Wh $kg^{-1}$ at 100 W $kg^{-1}$ | 10 kW $kg^{-1}$ at 43.7 Wh $kg^{-1}$ | 84% after 10000 cycles at 2 A $g^{-1}$ 0-4 V | 12 |
| S-C-N//NPCP | 200 Wh $kg^{-1}$ at 450 W $kg^{-1}$ | 22.5 kW $kg^{-1}$ at 68.7 Wh $kg^{-1}$ | 44% after 4000 cycles at 2 A $g^{-1}$ 0.5-4 V | 6 |
| $MoSe_2$-$TiO_{2-x}$-G//AC | 109 Wh $kg^{-1}$ at 100 W $kg^{-1}$ | 8 kW $kg^{-1}$ at 64 Wh $kg^{-1}$ | 88% after 3000 cycles at 2 A $g^{-1}$ 0.5-3.5 V | 13 |
| PCNS//HPC | 119 Wh $kg^{-1}$ at 200 W $kg^{-1}$ | 20 kW $kg^{-1}$ at 53 Wh $kg^{-1}$ | 82% after 8000 cycles at 5 A $g^{-1}$ 0-4 V | 7 |
| OMC//N-OMC | 119 Wh $kg^{-1}$ at 75 W $kg^{-1}$ | 5.8 kW $kg^{-1}$ at 33 Wh $kg^{-1}$ | 73% after 1800 cycles at 1 A $g^{-1}$ 0-4 V | 8 |
| VP-VNO//AC | 120 Wh $kg^{-1}$ at 185 W $kg^{-1}$ | 1.05 kW $kg^{-1}$ at 88 Wh $kg^{-1}$ | 86% after 20000 cycles at 0.1 A $g^{-1}$ 0.1-3.8 V | 14 |
| $NiS_x$@PCM//AC | 99.3 Wh $kg^{-1}$ at 140 W $kg^{-1}$ | 1.0 kW $kg^{-1}$ at 80 Wh $kg^{-1}$ | / 1.0-3.8 V | 15 |

**References**


1. Z. Li, J. Jiang, X. Liu, Z. Zhu, J. Wang, Q. He, Q. Kong, X. Niu, J. S. Chen, J. Wang and R. Wu, *Small*, 2022, **18**, e2203495.
2. G. Kresse and J. Furthmüller, *Comp. Mater. Sci.*, 1996, **6**, 15-50.
3. R. Car and M. Parrinello, *Phys. Rev. Lett.*, 1985, **55**, 2471-2474.
4. J. P. Perdew, K. Burke and M. Ernzerhof, *Phys. Rev. Lett.*, 1996, **77**, 3865-3868.
5. P. E. Blochl, *Phys. Rev. B*, 1994, **50**, 17953-17979.
6. S. Li, J. Zhang, Y. Li, P. Fan and M. Wu, *Nano Res. Energy*, 2024, **3**, e9120098.
7. L. Zhang, J. Sun, H. Zhao, Y. Sun, L. Dai, F. Yao, Y. Fu and J. Zhu, *J. Power Sources*, 2020, **475**, 228679.
8. J. Li, B. Wang, T. Hu, Y. Wang, Z. Sun, C. Wang, D. Zhang, Z. Wang and F. Li, *J. Mater. Chem. A*, 2021, **9**, 3360-3368.
9. G. Zhang, L. Zhang, Q. Ren, L. Yan, F. Zhang, W. Lv and Z. Shi, *ACS Appl. Mater. Interfaces*, 2021, **13**, 31650-31659.
10. Y. Wang, X. Xu, Y. Wu, F. Li, W. Fan, Y. Wu, S. Ji, J. Zhao, J. Liu and Y. Huo, *Adv. Energy Mater.*, 2024, 2401833.
11. W. Feng, C. Meng, X. Guo, B. Wu, X. Sui and Z. Wang, *Adv. Energy Mater.*, 2024, **14**, 2400558.
12. X. Ren, Z. Ren, Q. Li, W. Wen, X. Li, Y. Chen, L. Xie, L. Zhang, D. Zhu, B. Gao, P. K. Chu and K. Huo, *Adv. Energy Mater.*, 2019, **9**, 1900091.
13. C. Liu, M. Zhang, X. Zhang, B. Wan, X. Li, H. Gou, Y. Wang, F. Yin and G. Wang, *Small*, 2020, **16**, e2004457.
14. W. Cheng, B. Wan, S. Xu, M. Zhang, R. Zeng, Z. Liu, C. Zhang, F. Yin, G. Wang and H. Gou, *ACS Appl. Mater. Interfaces*, 2020, **12**, 29218-29227.
15. S. Li, W. He, B. Liu, J. Cui, X. Wang, D.-L. Peng, B. Liu and B. Qu, *Energy Storage Mater.*, 2020, **25**, 636-643.